JOURNAL OF Materials CHEMISTRY

Porous zirconium phosphates prepared by surfactant-assisted precipitation

Y. Sun, P. Afanasiev,* M. Vrinat and G. Coudurier

Institut de Recherches sur la Catalyse, CNRS, 2 avenue Albert Einstein, 69626 Villeurbanne Cedex, France. E-mail: afanas@catalyse.univ-lyon1.fr

Received 2nd June 2000, Accepted 19th July 2000
First published as an Advanced Article 31st August 2000

Porous zirconium phosphates with surface areas in the range 400–500 $m^2\ g^{-1}$ have been prepared by aqueous precipitation in the presence of various surfactants, followed by thermal treatment at 773 K. Preparation conditions, including surfactant nature and concentration, type of precipitating agent and fluoride additives were found to have significant influence on the textural properties of the resulting solids. X-Ray diffraction showed that, before calcination, refluxed samples have an ordered lamellar structure which disappears upon oxidation of the surfactant. IR and ^{31}P MAS NMR spectroscopy indicate formation of P–O–P bonds due to condensation of phosphate groups during the heat treatment.

1 Introduction

Phosphates of main and transition group metals constitute an important class of inorganic materials widely studied in different fields of chemistry, including ion exchange,[1] high temperature ion conductivity,[2] and catalysis.[3,4] Phosphate-based porous materials have received considerable attention. For example, crystalline lamellar metal(IV) phosphates or phosphonates are used as the hosts for inorganic or organic species to form porous materials with pillared layered structures (PLS).[5,6] Another example is crystalline microporous aluminophosphates (AlPOs) with open framework structures.[7,8]

Recently, much effort has been devoted to the surfactant-assisted synthesis of mesoporous aluminophosphates,[9] using a synthetic approach similar to that used for the preparation of MCM mesoporous materials.[10,11] Syntheses of mesoporous vanadium phosphorous oxides (VPO) have also been attempted.[12,13] However, if mesostructured inorganic–surfactant composites are easily obtained with different transition metal compounds, the removal of surfactant without destroying mesoporosity often presents considerable difficulty.

Synthesis of zirconium and titanium oxides modified by phosphate groups, either through post-treatment[14,15] or using surfactants with phosphate headgroups,[16–18] can result in high surface area products. On the other hand, pure zirconium phosphates themselves are not known as mesoporous materials. Therefore, a method for the preparation of porous zirconium phosphates with high and stable surface areas could be of interest. In this paper, we report on a simple method for the preparation of high surface area porous zirconium phosphates by means of surfactant-assisted precipitation, as well as characterization of these solids.

2 Experimental

2.1 Preparation of solids

Zirconyl chloride octahydrate ($ZrOCl_2{\cdot}8H_2O$) was used as a zirconium precursor salt in all experiments. H_3PO_4, $NH_4H_2PO_4$ and $(NH_4)_2HPO_4$ were used as precipitating agents. Cetyltrimethylammonium chloride (CTAC), hexadecylamine (HDA) and sodium dodecyl sulfate (SDS) were chosen as typical cationic, neutral and anionic surfactants, respectively. All the reagents were high purity grade from Aldrich.

The preparation mode was different according to the surfactant type, since SDS forms a precipitate if mixed with a Zr salt solution. Therefore, in the case of cationic or neutral-type surfactants, a solution of the surfactant was mixed with the Zr salt, then the phosphorous salt was added, whereas, for SDS, the order of mixing was changed to avoid precipitation of Zr organic salt.

100 mL of 0.1 M $ZrOCl_2$ aqueous solution with or without addition of NH_4HF_2 (F/Zr molar ratio from 0 to 1) was mixed with 100 mL of 0.1 M aqueous CTAC (or ethanolic HDA), then 100 mL of a 0.3 M precipitating agent was added dropwise under vigorous stirring. For the anionic-type surfactant, SDS solution was mixed with the precipitating agent solution, then 100 mL of 0.1 M $ZrOCl_2$ was added dropwise. In all three cases using the different surfactants, the reaction mixtures were stirred under ambient conditions for 2 h. Then, aging of precipitates for 24 h at room temperature or refluxing for 12 h was carried out. After filtration and washing with water until the washing solution showed an absence of Cl^- and was of neutral pH, the precipitates were dried overnight at 383 K. The surfactants were removed by calcination, first under N_2 flow at 773 K for 5 h (heating rate 1.5 K min^{-1}), then for an additional 5 h under O_2 flow at 773 K. The products are denoted $ZrPS^X$, where $S^X = S^+$, S^0 and S^-; S^X refers to the particular surfactant, cationic, neutral or anionic, respectively, which was employed.

2.2 Characterization

Surface areas and pore size distributions were obtained by adsorption of N_2 at 77 K. Before measurement, all samples were evacuated at 623 K for 3 h. Calculations were done using the BET equation or *t*-curves. Microporosity distribution was studied using the Horvath–Kawazoe method.[20] X-Ray diffraction (XRD) patterns were recorded on a Siemens D500 diffractometer using Ni-filtered Cu-Kα radiation. For the small angle diffraction measurements, a 0.2 mm slit was used. ^{31}P NMR spectra were obtained on a Brucker MSL 300 instrument (ref. aq. H_3PO_4. MAS spectra (rotation frequency 12 KHz) were recorded with proton decoupling of the ^{31}P signal. Chemical analyses of phosphorus and zirconium were carried out using atomic emission methods with a Spectroflame ICPD apparatus. IR spectra were recorded in air with a Brucker spectrometer by diluting the samples (*ca.* 1 wt%) in KBr. High resolution transmission electron microscopy

 DOI: 10.1039/b004845n

(HREM) was done on a JEOL 2010 instrument, using a 200 kV accelerating voltage.

3 Results and discussion

3.1 Textural properties

The preparation conditions, textural properties and compositions of the samples studied in this work are summarised in Table 1. Fig. 1 depicts the isotherm shapes of selected solids. Below we discuss the influence of different parameters on the properties of the solid products.

3.1.1 Influence of surfactant nature. From the data listed in Table 1, it can be seen that using CTAC and HDA as surfactants results in high surface porous products, whereas the effect of SDS is poor. For example, after calcination in air, the surface areas of the CTAC and HDA-derived samples were, respectively, 519 ($ZrPS^+1$) and 504 $m^2\,g^{-1}$ ($ZrPS^0 1$), as compared to 108 $m^2\,g^{-1}$ ($ZrPS^-2$) for the SDS-derived solids. According to the chemical analyses, the amount of carbon in the non-calcined $ZrPS^-2$ sample is less than 1%, whereas the C contents in the $ZrPS^+1$ and $ZrPS^0 1$ solids are 30.4 and 24.2%, respectively. Low carbon content indicates that after washing, almost no surfactant remains in the $ZrPS^-2$ sample.

The TGA results are in agreement with the chemical analyses. Two weight loss peaks were observed upon heating in air (Fig. 2). The first, in the range 570–590 K, is due to the decomposition and burning of the surfactant (the sample becomes black), and the second maximum, at 710–740 K, is due to burning of carbonaceous organic residuals. The total weight loss measured at 823 K varied between 50 and 60 wt%.

Though the samples prepared with cationic and neutral surfactant ($ZrPS^+1$ and $ZrPS^0 1$) have nearly the same surface area, their pore structures are quite different, as follows from their dissimilar nitrogen adsorption–desorption isotherms [Fig. 1(b) and (d)]. The $ZrPS^+1$ sample shows a type IV-like isotherm with an H_2-type hysteresis loop, suggesting an ink bottle-type pore structure,[21] whereas the $ZrPS^0 1$ solid shows a type II isotherm with a hysteresis loop at high relative pressure, typical for large pores between the particles. $ZrPS^0 1$ possesses much higher pore volume and larger mean pore diameter than $ZrPS^+1$. Note that in Table 1, we give mean sizes for the

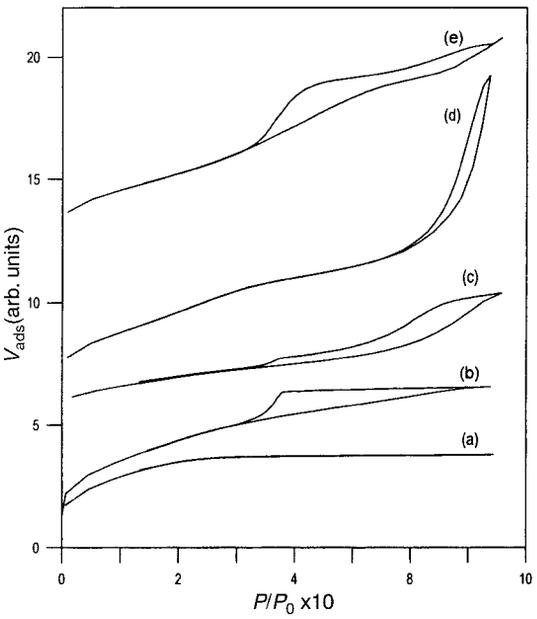

Fig. 1 N_2 adsorption–desorption loops for the samples $ZrPS^+6$ (a), $ZrPS^+1$ (b), $ZrPS^+3$ (c), $ZrPS^0 1$ (d) and $ZrPS^0 3$ (e).

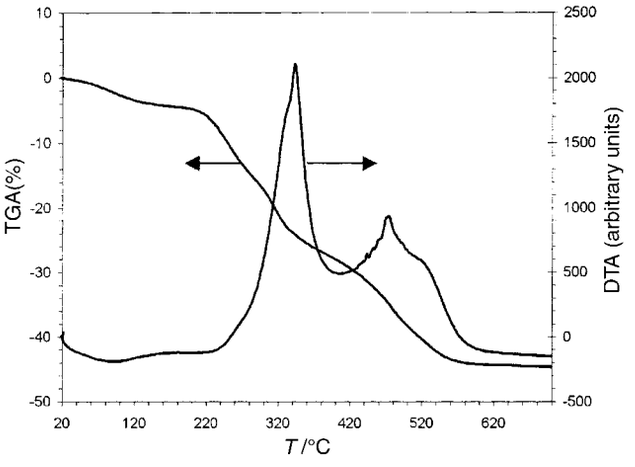

Fig. 2 TGA traces for the $ZrPS^0 1$ sample heated in air.

Table 1 Preparation conditions, textural properties and P/Zr ratios for the ZrPS solids

Sample	Preparation mode[a] X-Y-Z-W	S_t/$m^2\,g^{-1}$	S_{BET}/$m^2\,g^{-1}$	V_{tot}[b]/$cm^3\,g^{-1}$	V_m[c]/$cm^3\,g^{-1}$	V_m/V_{tot} (%)	D[c]/nm	P/Zr ratio[d]
$ZrPS^+1$	A-1-H2-0	502	519	0.36	0.23	63	3.3	2.1
$ZrPS^+2$	R-1-H2-0	463	479	0.35	0.25	71	3.1	2.1
$ZrPS^+3$	A-0.5-H2-0	(241)[e]	232	0.26	0.25	96	5.8	—
$ZrPS^+4$	A-1.5-H2-0	400	405	0.29	0.20	69	3.4	—
$ZrPS^+5$	A-1-H3-0	325	368	0.23	0.11	47	3.2	2.1
$ZrPS^+6$	A-1-H-0	310	415	0.21	0.03	14	2.8	1.4
$ZrPS^+7$	R-1-H2-0.01	(498)[e]	487	0.35	0.25	71	3.2	2.1
$ZrPS^+8$	R-1-H2-0.1	(366)[e]	351	0.30	0.28	93	3.3	2.1
$ZrPS^+9$	R-1-H2-1	199	199	0.23	0.23	100	3.6	2.0
$ZrPS^+10$	R-1-H-0	336	450	0.18	0.02	10	2.2	1.3
$ZrPS^0 1$	A-0.5-H2-0	(512)[e]	504	0.85	0.71	83	7.7	1.9
$ZrPS^0 2$	R-0.5-H2-0	(503)[e]	495	0.74	0.62	83	7.9	2.1
$ZrPS^0 3$	A-1-H2-0	(420)[e]	396	0.50	0.50	100	4.2	—
$ZrPS^0 4$	A-0.5-H3-0	(286)[e]	272	0.42	0.36	85	8.5	2.0
$ZrPS^0 5$	A-0.5-H-0	(511)[e]	504	0.67	0.56	83	6.3	1.2
$ZrPS^-1$	A-1-H3-0	—	4	—	—	—	—	1.9
$ZrPS^-2$	A-1-H2-0	(123)[e]	108	0.10	0.09	90	3.9	2.0
$ZrPS^-3$	A-1-H-0	—	7	—	—	—	—	1.6

[a]Designation of preparation mode X-Y-Z-W. X: R = reflux for 12 h; A = aging for 24 h. Y is the surfactant to Zr molar ratio. Z is the designation of the phosphate source: H3 = H_3PO_4; H2 = $NH_4H_2PO_4$; H = $(NH_4)_2HPO_4$. W is the F^- to Zr molar ratio in the reaction mixture. [b]Total pore volume (V_{tot}) determined by integration of the absorption curves. [c]Cumulative mesopore volume (V_m) and mean mesopore diameter (D) calculated using the Robert cylindrical pore model.[19] [d]Determined from the elemental analyses. [e]S_t put in parentheses when its measured value was greater than S_{BET} and, thus, overestimated.

mesopores, whereas the microporosity is characterised only by its relative volume. To characterise the microporosity, we conducted additional experiments with small increases in pressure and treated the isotherms using the Horvath–Kawazoe method. The pore size was 1.0–1.1 nm in all cases.

The $ZrPS^{+}2$ and $ZrPS^{0}2$ samples, prepared under reflux, show slightly lower surface areas compared to non-refluxed $ZrPS^{+}1$ and $ZrPS^{0}1$. However, they have similar isotherm shapes (not shown) to those of the $ZrPS^{+}1$ and $ZrPS^{0}1$ samples, respectively. The low surface area $ZrPS^{-}2$ sample also shows a type IV-like isotherm, having a similar form to that of $ZrPS^{+}1$.

We see, therefore, that the surfactant nature has crucial importance for the textural properties of the obtained zirconium phosphate. Cationic (CTAC) and neutral (HDA) surfactants strongly improve textural parameters, whereas anionic surfactant (SDS) showed a rather negative influence.

3.1.2 Influence of surfactant concentration. CTAC-derived $ZrPS^{+}1$ was prepared with a surfactant to Zr molar ratio of 1. To study the influence of the surfactant concentration on texture, we also prepared $ZrPS^{+}3$ and $ZrPS^{+}4$ samples having a surfactant to Zr ratio of 0.5 and 1.5, respectively. The data in Table 1 show that their surface areas are somewhat lower than that of the $ZrPS^{+}1$ sample. The isotherm for $ZrPS^{+}3$ changed to type II [Fig. 1(c)], while the isotherm for $ZrPS^{+}4$ remained type IV-like. A change in the isotherm type was also observed in HDA-derived samples on increasing the surfactant to Zr ratio from 0.5 ($ZrPS^{0}1$) to 1 ($ZrPS^{0}3$). The latter has a type IV isotherm with a H_2 hysteresis loop [Fig. 1(e)], as opposed to the type II isotherm of the former. At the same time, according to the thermal analysis, the amount of surfactant retained by the solid increased from 27 to 43 wt%.

3.1.3 Influence of precipitating agent. The nature of the precipitating agent might be very important, since it determines the mechanism and kinetics of reactions and, as a consequence, has a decisive impact on the chemical composition and structure of the precipitate. Three different phosphate sources have been tried in this work, aqueous phosphoric acid and two ammonium phosphate salts.

We observed that the nature of the precipitating agent influenced both the chemical composition of the solid precipitates and their textural properties. The most basic precipitating agent, $(NH_4)_2HPO_4$, yields products with decreased P/Zr ratios (1.4, 1.2 and 1.6 for the samples $ZrPS^{+}6$, $ZrPS^{0}5$ and $ZrPS^{-}3$, respectively), as compared to ratios close to 2 in all the other cases (except for $ZrPS^{+}10$). This observation can be explained by hydrolysis of Zr–O–P bonds due to the increased pH of the reaction mixture, which is in the range of 7–8 when using $(NH_4)_2HPO_4$ (compared to less than 1 and about 3 for H_3PO_4 and $NH_4H_2PO_4$, respectively).

The pore size and volume are also strongly affected by the nature of the precipitating agent. H_3PO_4-precipitated $ZrPS^{+}5$ and $ZrPS^{0}4$ samples have somewhat decreased surface areas (Table 1). High surface area $ZrPS^{0}5$, obtained with $(NH_4)_2HPO_4$ and ethanolic HDA, provides similar isotherm patterns to the corresponding $NH_4H_2PO_4$-derived solids. However, CTAC-templated $ZrPS^{+}6$ precipitated with $(NH_4)_2HPO_4$ and with a high surface area of 415.6 $m^2\ g^{-1}$ is quite different from the others, showing a type I isotherm virtually without hysteresis [Fig. 1(a)], a feature usually seen for microporous materials. The volume of micropores, deduced from a *t*-plot curve, was 0.20 $cm^3\ g^{-1}$, close to the value of V_{tot} (0.21 $cm^3\ g^{-1}$). At the same time, V_m/V_{tot} is as low as 14%.

3.1.4 Influence of F^- admixtures. Fluoride is known to strongly affect formation of zirconium phosphates in aqueous solutions, probably because of strong complexation between F^- ions and Zr(IV) species. F^- may have a pronounced effect on improving the crystallinity of lamellar zirconium phosphates and zeolites.[22] Therefore, we studied the influence of F^- on the properties of refluxed samples. As can be seen from the data in Table 1, ($ZrPS^{+}2$, $ZrPS^{+}7$, $ZrPS^{+}8$ and $ZrPS^{+}9$ samples), when the F^-/Zr ratio increases from 0 to 1, the surface area decreases from 479.5 to 199.2 $m^2\ g^{-1}$. As follows from these data, an admixture of F^- has a negative effect on the specific surface area. Pore size was affected only slightly, increasing from 3.1 to 3.6 nm. At the same time, mesoporosity share increases, with V_m/V_{tot} rising from 71 to 100%. The isothermal patterns of these samples remain of type IV, similar to $ZrPS^{+}1$, indicating that no qualitative change in the pore structure occurs. We suggest that fluoride increases the velocity of precipitate aging during reflux, which is known to produce an increase in porosity simultaneously with some decrease in the surface area.[23]

Summarizing the data presented above, we can state that the new zirconium phosphate materials we prepared have high and stable surface areas and develop considerable mesoporosity. Their texture can be controlled by varying the synthesis conditions (extent of aging and surfactant nature), as is the case with mesoporous silica.[24,25]

In the next sections, physico-chemical characterizations are described to provide some insight into the structure of these solids.

3.2 XRD patterns and HREM images

After calcination at 773 K, all the samples were totally amorphous. The absence of peaks in the low angle range indicates that there is no ordered arrangement of pores in these materials. Some ordering could only be found in the non-calcined specimens. In Fig. 3, XRD patterns of surfactant-containing uncalcined samples prepared by refluxing are shown. Low angle peaks at interplanar distances of *ca.* 4.9 and 3.1 nm for $ZrPS^{+}10$ and $ZRPS^{0}2$ indicate the formation of the ordered surfactant–zirconium phosphate phases, in which Zr–P layers are apparently separated by surfactant molecules. This ordered structure exists only in refluxed samples and was not formed in the precipitates obtained by aging under ambient conditions. Presumably, the first XRD peak is the (001) reflection of the lamellar ordered structure whereas the small

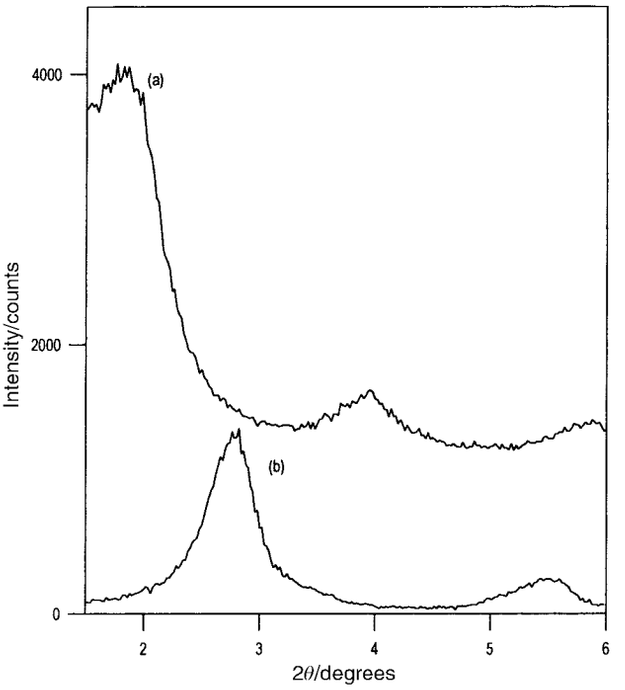

Fig. 3 XRD patterns of the uncalcined samples: $ZrPS^{+}10$ (a) and $ZrPS^{0}2$ (b).

peak at half distance (2.5 and 1.6 nm) is due to the (002) group of planes.

Although the low angle XRD lines are too broad and weak to elucidate the structure of the ordered phases, HREM studies clearly reveal lamellar ordering. CTAC-derived samples after reflux were homogeneous at the nanometer scale (15 nm EDAX spot analysis) and showed a mean P/Zr ratio of 1.95, close to that determined by chemical analysis. Smooth distorted layers were observed (Fig. 4). The approximate interlayer distance values (*ca.* 4.8 and 3.0 nm for $ZrPS^{+}10$ and $ZRPS^{0}2$, respectively) were close to the distances calculated from low angle XRD.

HREM confirms the hypothesis that hydrolysis occurred in the solids precipitated using dibasic ammonium phosphate. The $ZrPS^{+}10$ sample, refluxed in basic solution, was strongly heterogeneous, according to EDAX analysis. Moreover, it showed the presence of ZrO_2 spherical particles of *ca.* 20 nm size (Fig. 5). Formation of ZrO_2 due to hydrolysis is consistent with the decreased P/Zr ratio found by chemical analysis (Table 1). The possibilities of ordering using reflux in basic solutions are therefore limited for Zr phosphates as compared to MCM silicas.

3.3 Infrared spectroscopy

IR spectra of selected samples were obtained from KBr discs. Comparison of the IR spectra before and after calcination shows that absorption bands around 1477 and 2800–3000 cm^{-1} due to C–H stretching disappear after calcination, due to removal of the surfactants. New bands at *ca.* 750 cm^{-1} appear, which can be ascribed to P–O–P vibrations.[26] In the P–O stretching region (1000–1100 cm^{-1}), a shift of *ca.* 55–65 cm^{-1} towards higher wavenumbers occurs after calcination, suggesting that the P–O bonds in the tetrahedra become more covalent. For the calcined samples, a broad unresolved peak was seen in the range 3600–3200 cm^{-1}, characteristic of OH groups with considerable hydrogen bonding. Evolution of this signal from sample to sample was weak and insufficient to enable any conclusions to be drawn.

3.4 ^{31}P MAS NMR spectroscopy

The chemical shifts and relative intensities of ^{31}P MAS NMR peaks are summarised in Table 2 for the samples calcined at 773 K. Four resonances can be distinguished in different samples. Comparing our data with that in the literature, we can attribute the observed signals around −5, −12 and −18 to −20 ppm to phosphorus atoms with one, two and three P–O–Zr bonds, respectively (Table 2). The higher the chemical shift of the ^{31}P signal, the greater the number of Zr–O–P bonds. The signals in the range *ca.* −28–30 ppm indicate formation of P–O–P bonds. The gradual decrease in the chemical shift corresponds to progressive deprotonation and subsequent condensation of phosphate species during calcination. Segawa and co-workers[26,27] have shown by IR and ^{31}P MAS NMR spectroscopy that phosphate groups in different zirconium phosphates (ZrP gel, α-ZrP and ε-ZrP) condense gradually to form P–O–P bonds with increasing temperature. The ZrP gel, after evacuation at 773–1073 K, was regarded as an XRD amorphous zirconium diphosphate.[27] From Table 2, we can see that such a ZrP gel treated at 773 K shows similar chemical shifts to high field resonance in our samples. The FT-IR results discussed above also suggest the presence of some P–O–P bonds (750 cm^{-1}). Therefore, we conclude that the resonances at 28–30 ppm are due to a certain amount of P–O–P bonds. It can be further inferred from a comparison of relative intensities of peaks that the degree of condensation is decreased due to the presence of surfactants. Indeed, in the case of the non-templated solids, calcination under the same conditions led to crystalline ZrP_2O_7, with the spectrum showing only high field P–O–P signals. Low field signals at −5 and −12 ppm are probably due to protonated phosphate groups. They are most intense in the initial non-calcined solids and disappear progressively upon calcination, together with the elimination of water. The presence of organic templates retards this process. We suggest that lower Zr–P layer packing density and interaction with organic residuals hinders the interactions of protonated phosphate groups which are necessary to eliminate water and produce pyrophosphate.

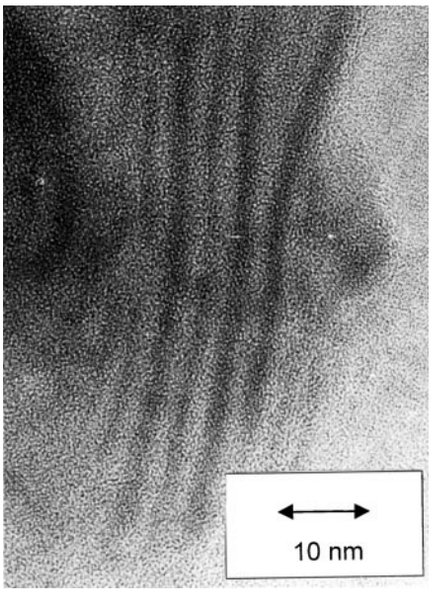

Fig. 4 HREM photo of the uncalcined sample $ZrPS^{+}1$.

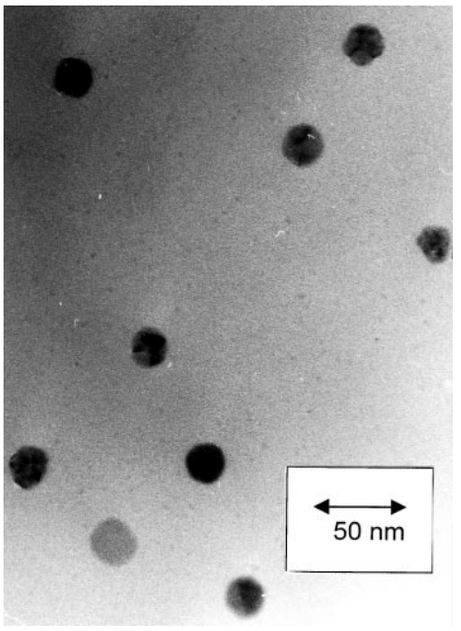

Fig. 5 HREM photo of the uncalcined sample $ZrPS^{+}10$.

4 Conclusions

In this work we describe the surfactant-assisted preparation of amorphous zirconium phosphates possessing high surface areas and considerable pore volume in the mesopore range. Such solids may be of particular interest as catalytic supports. For example, zirconium phosphates used as supports for hydrotreating catalysts recently reported by Ziyad *et al.*[28] have surface areas of *ca.* 100 $m^2\,g^{-1}$. The solids prepared in the present work provide surface areas several times greater

Table 2 Parameters of the ^{31}P MAS NMR spectra of selected ZrPS samples

Sample	Chemical shift (ppm) and relative amount (%) in parentheses			
	$(Zr–O)PO_3$	$(ZrO)_2PO_2$	$(Zr–O)_3PO$	P–O–P
$ZrPS^+1$	—	—	−21.1 (44)	−30.3 (56)
$ZrPS^+2$	—	−12.5 (11)	−20.0 (36)	−29.0 (53)
$ZrPS^+6$	—	—	−19.0 (50)	−27.9 (50)
$ZrPS^+8$	−5.8 (3)	−12.7 (14)	−20.5 (37)	−28.6 (46)
$ZrPS^0 1$	—	—	−18.2 (53)	−30.1 (47)
$ZrPS^0 2$	−5.6 (14)	−12.5 (23)	−20.9 (26)	−29.3 (37)
ZrP-gel[26] (calc. 773 K)	—	—	−19.2 (29)	−28 (71)

(typically 400–500 $m^2 g^{-1}$ after 773 K calcination). Therefore, the materials described here present may well be useful for supporting sulfides. Additionally, they could be used to support active phases for acid–base or partial oxidation catalysis. The role of surfactant in the stabilisation of the high surface area of these materials seems to be to act as scaffolding and preserve the loose packing of the Zr–P layers, rather than the ordered honeycomb structure which would otherwise result.

Acknowledgements

Y. S. would like to express personal gratitude to Prof. J.C. Vedrine for his help in obtaining financial support for a postdoctoral fellowship.

References

1 *Inorganic Ion Exchange Materials*, ed. A. Clearfield, CRC Press, Boca Raton, 1982, ch. 1–3.
2 J. B. Goodenough, H. Y. P. Hong and J. A. Kafalas, *Mater. Res. Bull.*, 1976, **11**, 203.
3 A. Clearfield and D. S. Thakur, *Appl. Catal.*, 1986, **26**, 1.
4 J. B. Moffat, *Catal. Rev. Sci. Eng.*, 1978, **18**(2), 199.
5 P. Olivera-Pastor, P. Maireles-Torres, E. Rodriguez-Castellon and A. Jimenez-Lopez, *Chem. Mater.*, 1996, **8**, 1758.
6 A. Clearfield, *Chem. Mater.*, 1998, **10**, 2801.
7 S. T. Wilson, B. M. Lok, C. A. Messina, T. R. Cannon and E. M. Flanigan, *J. Am. Chem. Soc.*, 1982, **104**, 1146.
8 *Synthesis of Microporous Materials*, ed. M. L. Occelli and H. Robson, Van Nostrand Reinhold, New York, 1992, pp. 240–349.
9 T. Kimura, Y. Sugahara and K. Kuroda, *Microporous Mesoporous Mater.*, 1998, **22**, 115.
10 J. S. Beck, J. C. Vartuli, W. J. Roth, M. E. Leonowicz, C. T. Kresge, K. D. Schmitt, C. T.-W. Chu, D. H. Olson, E. W. Sheppard, S. B. McCullen, J. B. Higgins and J. L. Schlenker, *J. Am. Chem. Soc.*, 1992, **114**, 10834.
11 J. Y. Ying, C. P. Mehnert and M. S. Wong, *Angew. Chem., Int. Ed.*, 1999, **38**, 56.
12 T. Abe, A. Taguchi and M. Iwamato, *Chem. Mater.*, 1995, **7**, 1429.
13 T. Doi and T. Miyake, *Chem. Commun.*, 1996, 1635.
14 U. Ciesla, S. Schacht, G. D. Stucky, K. K. Unger and F. Schüth, *Angew. Chem., Int. Ed. Engl.*, 1996, **35**, 541.
15 M. Thieme and F. Schüth, *Microporous Mesoporous Mater.*, 1999, **27**, 193.
16 D. M. Antonelli and J. Y. Ying, *Angew. Chem., Int. Ed. Engl.*, 1995, **34**, 2014.
17 G. Pacheco, E. Zhao, A. Garcia, A. Sklyarov and J. J. Fripiat, *Chem. Commun.*, 1997, 491.
18 M. S. Wong and J. Y. Ying, *Chem. Mater.*, 1998, **10**, 2067.
19 B. F. Roberts, *J. Colloid Interface Sci.*, 1967, **23**, 266.
20 G. Horvath and K. Kawazoe, *J. Chem. Eng. Jpn.*, 1983, **16**, 470.
21 S. J. Gregg and K. S. W. Sing, *Adsorption, Surface Area and Porosity*, Academic Press, London, 1982.
22 G. Alberti and E. Torracca, *J. Inorg. Nucl. Chem.*, 1968, **30**, 317.
23 C. J. Brinker and G. W. Scherer, *Sol-gel science: the physics and chemistry of sol-gel processing*, Academic Press Inc, London and New York, 1990, p. 357.
24 C. Okkerse, in *Physical and Chemical Aspects of Adsorbents and Catalysis*, ed. B. G. Linsen, Academic Press, London, 1970, pp. 213.
25 V. A. Fenelonov, V. Yu. Gavrilov and L. G. Simonova, *Stud. Surf. Sci. Catal.*, 1983, **16**, 665.
26 K. Segawa, Y. Kurusu, Y. Nakajima and M. Kinoshia, *J. Catal.*, 1985, **94**, 491.
27 K. Segawa and Y. Nakajima, *J. Catal.*, 1986, **101**, 81.
28 M. Ziyad, M. Rouini and J. L. Portefaix, *Appl. Catal.*, 1999, **183**, 93.